In situ endoscopic observation of higher-order mode conversion in a microwave mode converter based on an electro-optic probe system

Ingeun Lee,[1] Dong-Joon Lee,[3,4,*] and EunMi Choi[1,2,4,5]

[1]*Department of Electrical Engineering, Ulsan National Institute of Science and Technology (UNIST), Ulsan 689-798, South Korea*

[2]*Department of Physics, Ulsan National Institute of Science and Technology (UNIST), Ulsan 689-798, South Korea*
[3]*Division of Physical Metrology, Korea Research Institute of Standards and Science (KRISS), Daejeon 305-340, South Korea*

[4]*These authors contributed equally.*
[5]*emchoi@unist.ac.kr*
[*]*dongjoonlee@kriss.re.kr*

Abstract: Visualizing the electromagnetic field transformation inside a microwave mode conversion region has been considered to be only realizable by simulation studies. For the first time, we present a comprehensive experimental observation of the electric field transformation occurring inside a metallic waveguide TE_{01}-to-TE_{02} mode converter. An efficient electro-optic (EO) probe and its associated probing system were used for measuring the electric field pattern in the external near-field region as well as in the internal and penetrated region of the mode converter. Utilizing the optically measured field patterns at the aperture of the mode converter, the conversion performance from the TE_{01} mode to the TE_{02} mode can be also evaluated. Experimentally measured field patterns near the apertures show excellent agreement with simulation data. The mode conversion to the next higher-order mode (TE_{01} to TE_{02}) was experimentally demonstrated with phase-stabilized and field-animated post processing. The presented in situ endoscopic photonic measurement technique for the field evolution inside a semi-enclosed structure could be used for visually inspecting manufacturing errors in fabricated structures, and could be of great interest for research on higher-order mode formation and transmission.

OCIS codes: (120.4290) Nondestructive testing; (120.4630) Optical inspection; (230.2090) Electro-optical devices; (230.7020) Traveling-wave devices; (350.4010) Microwaves.

References and links

1. M. Thumm, "Progress in gyrotron development," Fusion Eng. Des. **66-68**, 69–90 (2003).
2. J. Jin, M. Thumm, B. Piosczyk, S. Kern, J. Flamm, and T. Rzesnicki, "Novel numerical method for the analysis and synthesis of the fields in highly oversized waveguide mode converters," IEEE Trans. Microw. Theory Tech. **57**(7), 1661–1668 (2009).
3. S. G. Tantawi, R. J. Loewen, C. D. Nantista, and A. E. Vlieks, "The generation of 400-MW RF pulses at X-band using resonant delay lines," IEEE Trans. Microw. Theory Tech. **47**(12), 2539–2546 (1999).
4. M. Yeddula, S. Tantawi, J. Guo, and V. Dolgashev, "An analytic design and analysis method for a high-power circular to rectangular waveguide mode converter and its applications," IEEE Trans. Microw. Theory Tech. **57**(6), 1516–1525 (2009).
5. K. H. Kim, M. S. Choe, W. S. Lee, J. H. So, and E. M. Choi, "Near-field pattern of large aperture higher order mode generator using backpropagated fields in free space," IEEE Trans. Plasma Sci. **42**(4), 937–943 (2014).
6. K. Yang, G. David, S. Robertson, J. F. Whitaker, and L. P. B. Katehi, "Electrooptic mapping of near-field distributions in integrated microwave circuits," IEEE Trans. Microw. Theory Tech. **46**(12), 2338–2343 (1998).
7. D. J. Lee, J. Y. Kwon, and N. W. Kang, "Field analysis of electro-optic probes for minimally invasive microwave sampling," Opt. Express **22**(3), 2897–2909 (2014).
8. D. J. Lee, N. W. Kang, J. H. Choi, J. Y. Kim, and J. F. Whitaker, "Recent advances in the design of electro-optic

#223325 - $15.00 USD Received 17 Sep 2014; revised 21 Oct 2014; accepted 22 Oct 2014; published 30 Oct 2014

sensors for minimally destructive microwave field probing," Sensors (Basel) **11**(12), 806–824 (2011).
9. H. Togo, N. Shimizu, and T. Nagatsuma, "Near-field mapping system using fiber-based electro-optic probe for specific absorption rate measurement," IEICE Trans. Electron. **E90-C**(2), 436–442 (2007).
10. J. Valdmanis and G. Mourou, "Subpicosecond electro-optic sampling: Principles and applications," IEEE J. Quantum Electron. **22**(1), 69–78 (1986).
11. J. A. Valdmanis, "1 THz-bandwidth probe for high-speed devices and integrated circuits," Electron. Lett. **23**(24), 1308–1310 (1987).
12. M. Shinagawa and T. Nagatsuma, "An automated electro-optic probing system for ultra-high-speed IC's," IEEE Trans. Instrum. Meas. **43**(6), 843–847 (1994).
13. S. Wakana, T. Ohara, M. Abe, E. Yamazaki, M. Kishi, and M. Tsuchiya, "Fiber-edge electrooptic/magnetooptic probe for spectral-domain analysis of electromagnetic field," IEEE Trans. Microw. Theory Tech. **48**(12), 2611–2616 (2000).
14. S. Jawla, J. P. Hogge, S. Alberti, T. Goodman, B. Piosczyk, and T. Rzesnicki, "Infrared measurements of the RF output of 170-GHz/2-MW coaxial cavity gyrotron and its phase retrieval analysis," IEEE Trans. Plasma Sci. **37**(3), 414–424 (2009).
15. A. Garzarella, S. B. Qadri, and D. H. Wu, "Optimal electro-optic sensor configuration for phase noise limited, remote field sensing applications," Appl. Phys. Lett. **94**(22), 22113 (2009).
16. M. S. Choe and E. M. Choi, "Experimental study of TE_{01}-TE_{02} mode converter on 28 GHz," in *Proceedings of the Korean Physical Society* (Plasma, 2013), poster P2–H006.
17. A. Dandridge and A. B. Tveten, "Phase compensation in interferometric fiber-optic sensors," Opt. Lett. **7**(6), 279–281 (1982).

1. Introduction

In research with high-power and coherent microwave radiation at millimeter-scale wavelengths, the delivery of the radiation field has been an important concern. Continuous power in the megawatt- and millimeter- wave ranges can be available from modern gyrotron sources [1]. Gyrotrons and their unique transmission systems are particularly crucial for applications like plasma heating for nuclear science or active denial systems for military applications. The transmission waveguides associated with gyrotrons are usually over-sized corrugated metallic structures that help to generate the higher-order modes for low-loss coupled-mode conversion [2]. High power RF system is used to accelerate the particle in accelerator system in which the RF wave is manipulated to be pulse-compressed, combined and transmitted in a waveguide to couple to a RF cavity [3, 4]. One has to do special care to prevent breakdown in the transmission line system and the RF cavity. Therefore, breakdown test and computer simulation is crucial to understand the structure although the experimental proof is often time very costly and the simulation has limitation in representing the experimental device.

However, the measurement of electric field patterns from radiation sources in the power transmission region becomes more challenging as the radiation frequency increases, thus the waveguide structure decreases accordingly [5]. Furthermore, mode conversion and transformation occurring at irregular geometrical shape are virtually impossible to monitor directly with a conventional metallic probe since the probe considerably disturbs the field pattern inside or in the vicinity of the aperture of the structure. Moreover, in higher-order modes it is nontrivial to identify the mode structure from the measured field pattern, which can be considerably altered as the field diverges rapidly toward free space and diffracts at the metal boundaries. Consequently, the measurement of the field pattern in the extreme near-field region is necessary to verify the specific modes generated from higher-order mode generating structures or antennas. Therefore, a probe that causes less field perturbation and provides higher resolution in the near-field region is highly desired [6–10].

Electro-optic (EO) sensing technologies have been increasingly promoted for sensing electric fields in a significantly less invasive way since EO crystals can be fairly transparent to both the optical and electromagnetic spectra of interest [11–13]. This property enables the probe to explore blind zones of near-electric field distributions of radio frequency radiators [9]. Because of its non-metallic composition and its small size, we propose the EO probe for the investigation of higher-order mode electric fields at the very near the aperture of the radiator (or mode converter). Furthermore, we have adapted the EO probe to monitor the field

#223325 - $15.00 USD Received 17 Sep 2014; revised 21 Oct 2014; accepted 22 Oct 2014; published 30 Oct 2014

variations farther inside the radiation structure, which has not been possible with existing technologies. EO probing allows the monitoring of complex field patterns with high resolution and accuracy and can help the understanding of mode conversion phenomena. It can be an excellent tool for the inspection of structural defects by direct observation with electromagnetic (EM) waves; this can bring new insights to the microwave community, which requires precise EM-propagation prediction without disturbing the original pattern. In this paper, we present a comparison study between field pattern data simulated with the commercial code CST Microwave Studio™ (CSTMWS™) and experimental results [14]. First, the electrical and photonic probes, including the overall sensing system, are compared. Subsequently, the characteristics of the mode converter and its two distinct TE_{01}/TE_{02} mode patterns, as well as the field evolution between the modes throughout the converter, will be presented. Finally, the suitability of the EO-probe system for measuring the higher-order mode patterns will be discussed.

2. Experiment setup

Figure 1 shows the two different probes that were employed in the experiment: an EO probe and a commercial WR28 open-ended waveguide probe. The EO probe consists of an optical fiber, a dielectric support, a glass ferrule, and an EO crystal $LiTaO_3$ (1.5 mm x 1.5 mm x 0.5 mm). The detailed physical parameters, including the operation principle, of the probe can be found in our previous work [7, 8]. The WR28 open-ended waveguide probe was adapted for Ka-band (26.5–40 GHz) operation. Its cutoff frequency for the TE_{01} mode was 21.08 GHz, which was determined by the fixed dimensions of the waveguide aperture (7.11 mm x 3.56 mm). As shown in Fig. 1, the waveguide probe was significantly bulkier than the EO probe. Because of its compact size and minute sensing area, owing to the fiber-coupled scheme, the EO probe guarantees superior spatial resolution in comparison with the commercial WR28 open-ended waveguide. Moreover, the EO probe causes less field distortion than the metallic waveguide because it consists entirely of dielectrics, which are virtually transparent to the electromagnetic waves of interest [5, 15]. The EO-probe system was used to scan the electric fields not only for the analysis of the field patterns but also for the examination of the field evolution inside the mode converter. The measurements provided insight into the processes inside the mode converter structure and allowed the analysis of the electric field conversion in the corrugated geometry of the mode converter.

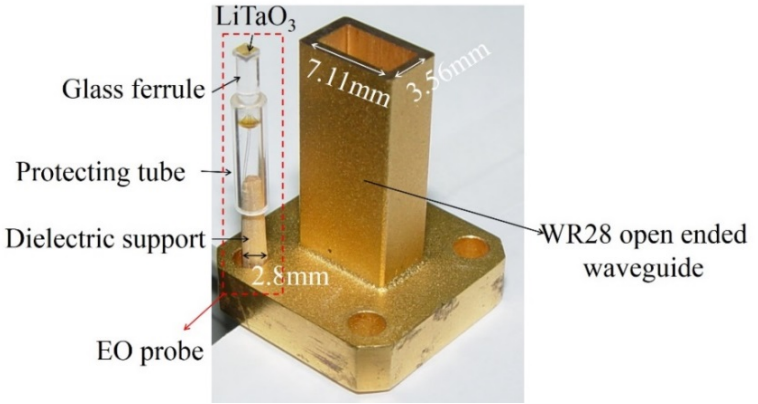

Fig. 1. The two different electric-field probes used in the measurements: the fabricated EO probe (left), and the commercial WR28 open-ended waveguide probe (right).

Waveguides with corrugated geometry are widely used when high-power and low-loss transmission at the millimeter-wavelength regime becomes a paramount concern. Modern gyrotrons are able to generate up to megawatt-scale power in millimeter-scale wavelengths

#223325 - $15.00 USD Received 17 Sep 2014; revised 21 Oct 2014; accepted 22 Oct 2014; published 30 Oct 2014

and the RF source for accelerator system generates even higher power level. Oversized waveguides are generally preferred for the delivery of such power in order to weaken the field intensity within the waveguides. However, oversizing breaks the single-mode condition and consequently higher-order modes emerge. These modes are usually orthogonal for straight waveguides and thus multiple modes can co-exist independently. As waveguides contain discontinuities, the orthogonality of the modes degrades and they begin to interact. The interaction between modes is determined by the shape, depth, period, and number of discontinuities and the coupling effect can be controlled depending on the periodic structure of the discontinuity. The modes can periodically transfer their energy and, by optimizing the corrugated structure, the energy exchange between modes can be maximized. This scheme enables high power to be effectively delivered with smaller risk of failure. We designed an efficient TE_{01}-to-TE_{02} mode converter operating at 28 GHz. The optimally corrugated radius ($\equiv a$) is expressed as $a = a_0 + a_1 \sin(2\pi z / \lambda_b)$ where a_0, a_1 and λ_b are the original radius, maximum radius of the corrugation, and beat wavelength, respectively. With no insertion and no wall loss condition, the conversion efficiency exceeds 92% when the number of periods (N) is 3, which corresponds to a mode converter length (l) 186 mm.

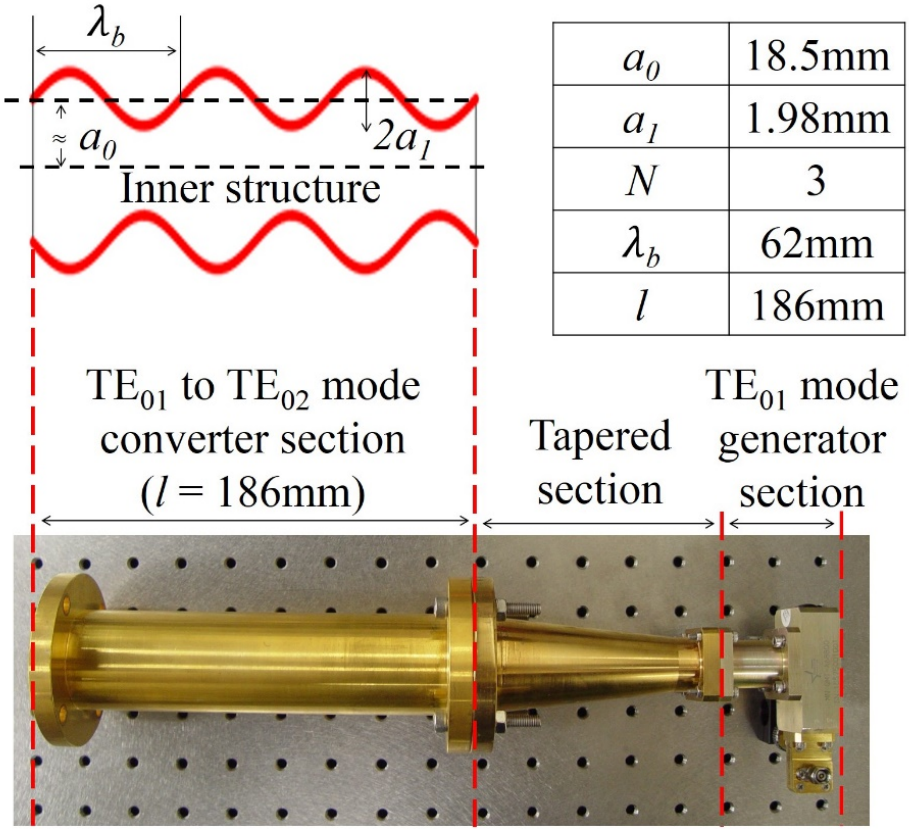

a_0	18.5mm
a_1	1.98mm
N	3
λ_b	62mm
l	186mm

Fig. 2. The oversized TE_{01}-to-TE_{02} mode converter set with corrugated geometry

The fabricated TE_{01}-to-TE_{02} mode converter, connected with the TE_{01} mode generator and the tapered section, is shown in Fig. 2. Each part affects the overall quality of the final TE_{02} mode pattern [16]. Experiments were performed to measure the extreme near-field pattern at the input and output sides of the converter aperture and the complete mode transformation inside the mode converter. The position of the EO probe was controlled by a programmable *x*-*y*-*z* translation stage for measuring field patterns at various regions.

#223325 - $15.00 USD Received 17 Sep 2014; revised 21 Oct 2014; accepted 22 Oct 2014; published 30 Oct 2014

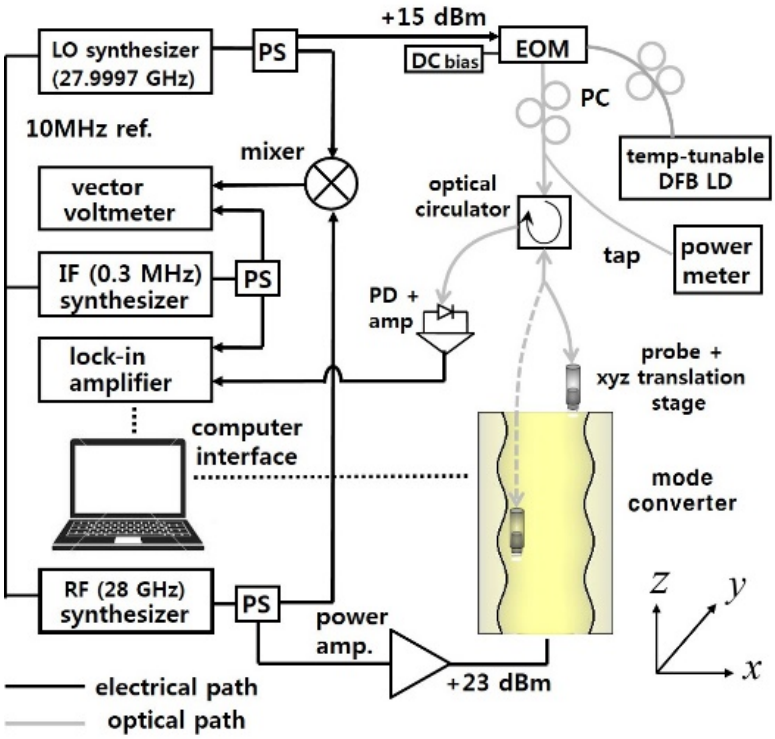

Fig. 3. Experimental schematic of the EO-probe system. (EOM: electrooptic modulator; DFB LD: distributed-feedback laser diode; PC: polarization controller; PS: power splitter; PD: photo diode; LO: local oscillator; IF: intermediate frequency). Mode pattern scans measured at 0.1 λ away from the mode converter's aperture (solid gray line) and inside the mode converter (dashed gray line).

In Fig. 3, the yellow structure represents the cross-sectional profile of the mode converter with the corrugated shape. The gray line denotes the optical-fiber path whereas the solid (or dashed) black line is the electrical (or synchronization) path. The IF synthesizer had an internal 10-MHz Rb clock that was used as a reference for all the interconnected synthesizers. The mode converter signal at 28 GHz was down-converted to a 0.3-MHz IF signal, which was subsequently decomposed into complex vector components. The magnitudes and phases of high-frequency vector signals (such as Ka-band) usually fluctuate and drift during lengthy scanning procedures. To correct the data for the phase and amplitude variations, we gathered these information at a vector voltmeter and send them to computer interface [17]. Special consideration was given to the following key factors of the experimental configuration of Fig. 3: the probe's length, the scan dimensions, the absence of any metallic component, and the mechanical balance of the device under test (DUT). Throughout this experiment, the dynamic field variation inside the mode converter could be monitored, allowing the analysis of the mode conversion area.

#223325 - $15.00 USD Received 17 Sep 2014; revised 21 Oct 2014; accepted 22 Oct 2014; published 30 Oct 2014

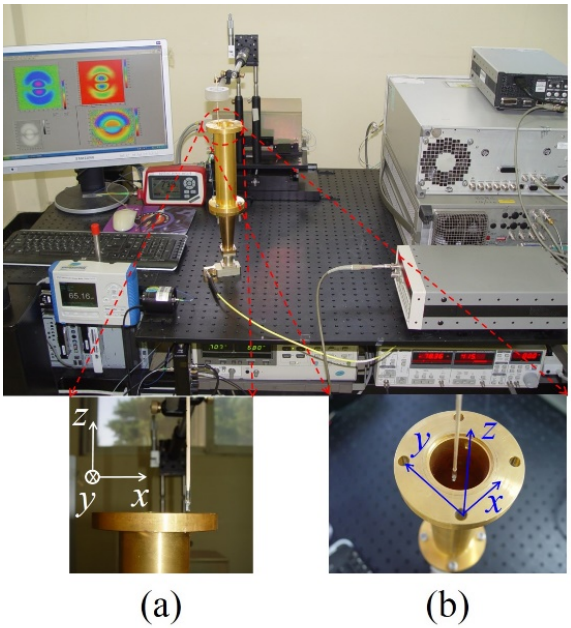

Fig. 4. Experimental setup of the two experiments: (a) mode pattern scan at 0.1 λ away from the mode converter's aperture; (b) mode pattern scan inside the mode converter

Figure 4 shows the experimental setup and the two different measurement layouts with the EO probe. The sensing scheme in Fig. 4(a) was used to measure two orthogonal TE_{01} and TE_{02} mode patterns in the *x*-*y* plane near the aperture of the converter. The configuration of Fig. 4(b) was implemented to measure the hybrid TE_{01}-TE_{02} mode in both *x*-*y* and *x*-*z* planes inside the converter. The EO probe was fabricated from *x*-cut $LiTaO_3$ wafer, which is positive uniaxial along the extraordinary refractive index (n_e). When an electric field is applied along the axis of n_e, this high electro-optic index is modified according to the field, and thus the laser polarization also becomes modulated. This means that the probe is sensitive to electric fields which are oriented in the same direction to the n_e axis (or optic-axis). We can utilize this feature to experimentally decompose two orthogonal field components and convert them to the radial field pattern.

3. Field measurement results and discussion

Figure 5 shows the TE_{01} mode patterns at the end of the tapered section of Fig. 2 and the comparison to the measured data. Figures 5(a)–5(c) represent TE_{01} mode pattern from CST MWS^{TM}, while Figs. 5(d)–5(f) and Figs. 5(g)–5(i) are originated from the EO probe and the metallic probe measuremnet, respectively. The asymmetric electric field pattern observed in Fig. 5(e) may result from a non-ideal TE_{01} mode pattern, originating from the low quality of the TE_{01} mode generator section that was purchased from a commercial supplier. In Fig. 5(i), the TE_{01} mode pattern from a Vector Network Analyzer (VNA) system shows asymmetric field distribution and lower-quality patterns than the EO probe mode patterns; this is due to reflected and scattered electric fields from the metallic open-ended waveguide and the tapered section's aperture. We also observed the same phenomenon in the TE_{02} mode pattern from the VNA data, as will be discussed in the next section.

#223325 - $15.00 USD Received 17 Sep 2014; revised 21 Oct 2014; accepted 22 Oct 2014; published 30 Oct 2014

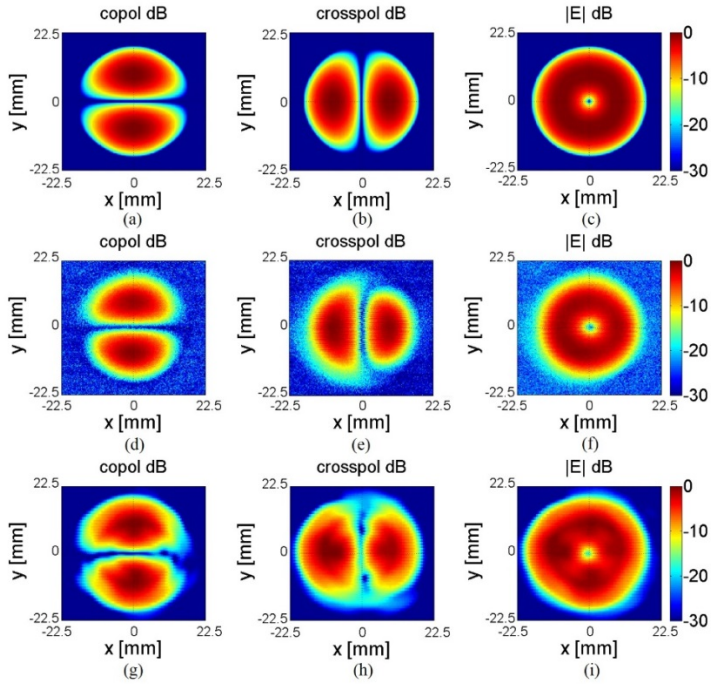

Fig. 5. TE_{01} mode patterns at the end of the tapered section: (a)–(c): simulation data; (d)–(f): EO-probe system measured data; (g)–(i): VNA measured data.

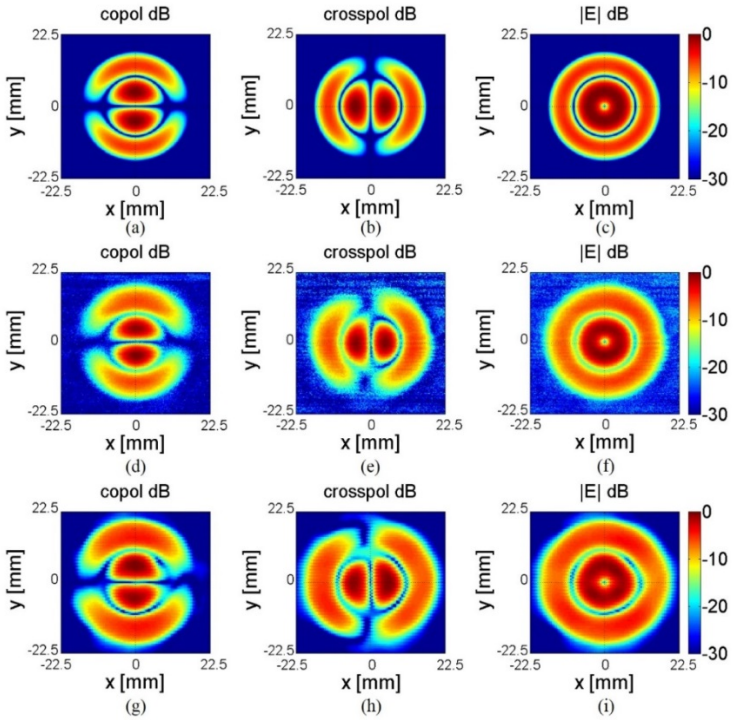

Fig. 6. TE_{02} mode pattern data from CST MWS^{TM} and the EO-probe system at 1-mm distance from its aperture: (a)–(c): Simulated data; (d)–(f): measured data; (g)–(i): VNA measured data. Each data set consists of 181✖ 181 pixels.

#223325 - $15.00 USD Received 17 Sep 2014; revised 21 Oct 2014; accepted 22 Oct 2014; published 30 Oct 2014

Figure 6 shows the field pattern results from the TE_{02} mode. Figures 6(a)–6(c) display simulated data from CST MWS^{TM}, whereas Figs. 6(d)–6(f) and Figs. 6(g)–6(i) are experimentally measured TE_{02} mode field patterns using the EO probe and the VNA, respectively. Each data set was acquired with every 0.025 wavelength of 28 GHz. Each E_x and E_y field in the EO-probe data was measured by simply turning the probe by 90 degrees. The cross-polarization feature of the probe exceeded 30 dB of the probe's dynamic range. Thus, we could superimpose the orthogonal fields to obtain the genuine radial patterns, as in Fig. 6(f). The experimentally measured field patterns are in excellent agreement with the simulation results; however, a mildly asymmetric field pattern was observed in the cross-polarization field results of Fig. 6(e), which originated from the low quality of the TE_{01} mode generator section, as previously discussed. As shown in Fig. 6, the EO-probe data show excellent sensing performance in the near-field. We defined a cross correlation function (CCF) to quantify the agreement between measurement and simulation as follows [14].

$$CCF = \sum_{i,j} u_r(i,j) u_m(i,j). \quad (1)$$

Here, u_r (i, j) is the modulus of the normalized reconstructed field amplitude and u_m (i, j) that of the normalized measured field amplitude. The CCF value between Figs. 6(c) and 6(f) is as good as 96%. On the other hand, the field patterns obtained by the VNA [Figs. 6(g), 6(h), and 6(i)] have larger sizes than those from the simulation and the EO probe owing to diffraction on the metal edges. Furthermore, irregular field intensity is also observed in the sum of the E-fields [Fig. 6(i)], which is not a real field pattern, as explained in the discussion regarding Fig. 5. The CCF value between Figs. 6(c) and 6(i) is 88.1%. The results establish that the EO-probe system causes less field perturbation than the conventional field-scanning method with a metal probe and has good resolution at the extreme near field regions. Additionally, we estimated the TE_{02} mode converter transmission efficiency (η) from the VNA and EO probe data and found the efficiencies η_{VNA} and η_{EO} to be 83.8% and 87%, respectively. During the RF signal transmission, an energy loss of −0.076 – −0.06dB resulted from insertion loss and wall loss. To investigate the dynamical behavior of the mode transformation endoscopically, the EO probe was inserted in the TE_{01}-to-TE_{02} mode converter section to measure the fields.

Figure 7(a) displays a cut-away view (*x*-*z* plane) of the scan of the mode converter section performed with a range of 24 mm x 179.75 mm. Due to the corrugated shape of the inner structure of the mode converter in the radial direction, the measurement plane was limited to the smallest inner radius, as shown in Fig. 7(a). We set the probe read one data point a second. This scanning speed was determined by considering the time constant of the lock-in amplifier and the time for the scanner position to settle from minute and transient vibrations of the probe. The scan image in Fig. 7(b) was composed of ~15500 data points with 0.05 λ spatial separation, which corresponds to approximately a 260-min-long scan. The field evolution can be categorized into the four zones indicated in Figs. 7(b) and 7(c). Figures 7(d) and 7(e) are phase information of the electric field inside the mode converter. The first zone (Zone I) is a pure TE_{01} mode and Zone II is the section of actual mode conversion. Zone III simultaneously purifies and intensifies the TE_{02} mode and the last zone (Zone IV) is a free-space propagation region. The asymmetry in the field intensity was again confirmed, especially in Zones II and III. The movie files contain a visual representation of the experimentally measured field propagation in the time domain inside the metallic mode converter by combining the measured amplitude and phase information; this is the first visualization of a minimally invasive endoscopic observation of the dynamical changes occurring during field formation. The field pattern in Fig. 7(b) illustrates the opposite phase information across the *z* axis. At the beginning and the end of the mode conversion zone (Zone II), we detected two prominent discontinuous field patterns that were not displayed in the simulation of Fig. 7(c). We also observed local discrepancies between measurement and

#223325 - $15.00 USD Received 17 Sep 2014; revised 21 Oct 2014; accepted 22 Oct 2014; published 30 Oct 2014

simulation in the *x-y* planes. The axial positions (*z* direction) of these unexpected field patterns were located from *z* = 81 mm to 83 mm and from 148 mm to 150 mm. Zone II is the critical region, where the mode radial number actually increases from 1 to 2; therefore, a slight variation in the axial position of the measurement plane may affect the result.

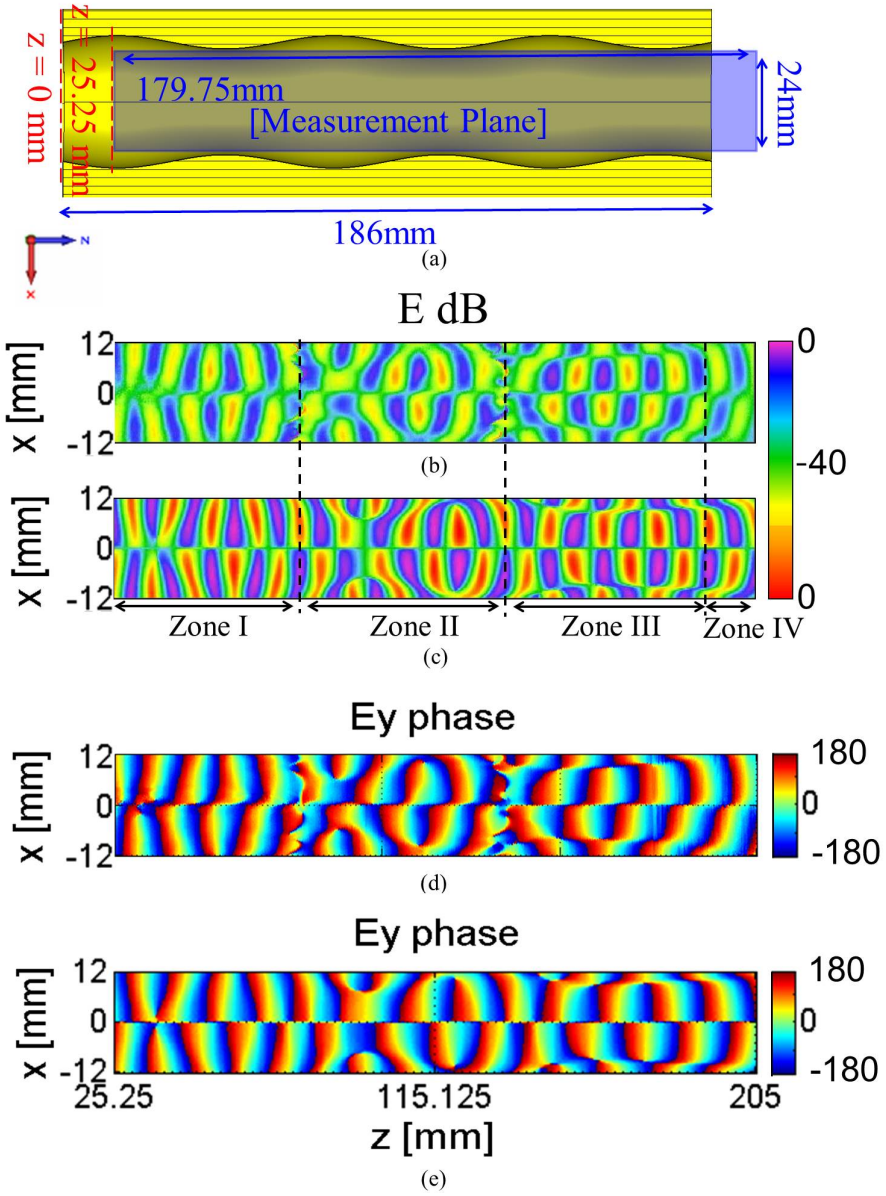

Fig. 7. Field patterns inside the mode converter: (a) measured plane of the mode converter; (b) measured E_y electric field intensity with phase information from the EO-probe system (Media 1); (c) simulated E_y electric field intensity with phase information from CST MWS (Media 2); (d) measured E_y field phase; (e) simulated E_y field phase.

In order to understand the discontinuity and the asymmetric field patterns observed in the experiment, we performed simulation studies. First of all, we verified that the EO probe does not cause the local field perturbation from the simulations. Secondly, in real situation, at Zone

#223325 - $15.00 USD Received 17 Sep 2014; revised 21 Oct 2014; accepted 22 Oct 2014; published 30 Oct 2014

I, non-ideal TE_{01} was introduced into the mode converter as shown in Fig. 5(f) and its mode purity obtained by EO probe system was 98.2%. Likewise, we artificially input the TE_{01} mode having 99.5% mode purity as shown in Fig. 8 and applied the asymmetric mode converter geometry in CSTMWS^{TM} for inspecting reasons of irregular field pattern shown in experimental data in Figs. 5–7.

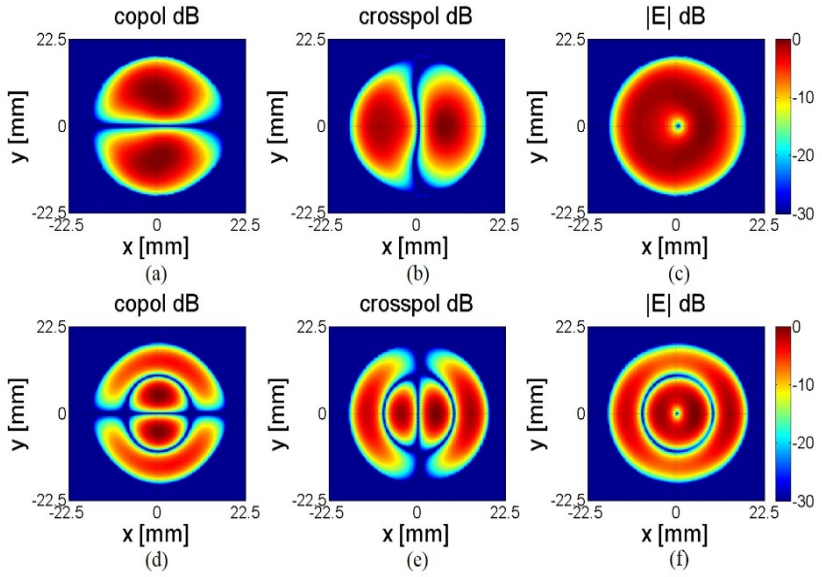

Fig. 8. TE_{02} field patterns from non-ideal TE_{01} in CST MWS^{TM}: (a)–(c) TE_{01} field pattern; (d)–(f) TE_{02} field pattern.

Figure 8 demonstrates that the symmetry in field patterns of the TE_{01} mode and TE_{02} mode was broken as the measured data in Figs. 5 and 6. From Fig. 8, we observed that non-ideal TE_{01} mode input described in Figs. 8(a)–8(c) and less than 1mm fabrication error in the simulations reproduced the irregular field pattern in Figs. 8(d)–8(f). From these results, we can conclude a combined error source from non-ideal TE_{01} mode at the first place and fabrication imperfection could lead to the overall field distortion in the *y* direction.

Although some discrepancy has been observed between simulation and experiment in the critical field-transforming zone, the endoscopic EO probing has been demonstrated to be suitable for the measurement of complex and dynamical field transformations.

4. Conclusions

We have demonstrated that highly complex mode patterns inside a waveguide can be characterized by minimally invasive photonic technology. The TE_{02} mode pattern was investigated at ~1 mm (0.1 λ) away from the aperture of a microwave mode converter and in its interior. This is the first time that an EO probe has been used to measure the internal mode patterns not only in the vicinity but also quite below the aperture of the structure. Excellent experimental results have been obtained using the EO field probe and the correlation between measured and simulated data was as good as 96.1%. Additionally, we have presented the first visualization of the mode conversion process occurring inside the higher-order mode converter. The proposed method may constitute a very promising approach to measuring higher-order mode formation more accurately and less invasively. The technique can find useful applications in the monitoring of manufacturing faults in delicate structures, such as a higher-order mode cavities, high performance antennas, mode transitions, and power combiners, by directly observing the electromagnetic wave transmission/conversion. The

#223325 - $15.00 USD Received 17 Sep 2014; revised 21 Oct 2014; accepted 22 Oct 2014; published 30 Oct 2014

proposed scheme can also be implemented for the study of high-power transmission lines for microwave, millimeter-wave, and THz-wave systems.

Acknowledgments

This work was supported by National R&D Program through the National Research Foundation of Korea (NRF) funded by the Ministry of Science, ICT & Future Planning (2014M1A7A1A03029874), the 2010 Research Fund (1.100008.01) of UNIST (Ulsan National Institute of Science and Technology and the KRISS (Korea Research Institute of Standards and Science) under the "Development of Technologies for Next-Generation Electromagnetic Wave Measurement Standards" project, grant 13011011. We wish to thank Mr. Sung Gug Kim and Mr. Mun Seok Choe at UNIST for helpful discussions of VNA experiments.

#223325 - $15.00 USD Received 17 Sep 2014; revised 21 Oct 2014; accepted 22 Oct 2014; published 30 Oct 2014